https://doi.org/10.3311/PPch.42388

Periodica Polytechnica Chemical Engineering

Hydrochar Derived from Zinc Chloride Aided Hydrothermal Co-carbonization of Sewage Sludge and Coconut Shells (*Cocos nucifera*)

Mark Joseph Arriola[1], Rose Francine Cantalejo[1], Mary Juriene Albert Perona[1], Faith Policarpio[1], Rugi Vicente Rubi[1,2*], Jerry Olay[1,2]

[1] Chemical Engineering Department, College of Engineering, Adamson University, 900 San Marcelino St., Ermita, 1000 Manila, Philippines
[2] Adamson University Laboratory of Biomass, Energy and Nanotechnology (ALBEN), Chemical Engineering Department, College of Engineering, Adamson University, 900 San Marcelino St., Ermita, 1000 Manila, Philippines
* Corresponding author, e-mail: rugi.vicente.rubi@adamson.edu.ph

Received: 02 October 2025, Accepted: 29 January 2026, Published online: 14 April 2026

Abstract

The hydrothermal co-carbonization (co-HTC) process is a promising method for improving the fuel properties of hydrochar. This process leverages synergistic interactions, facilitated by the Maillard reaction, which is believed to be catalyzed under acidic conditions. In this study, the co-HTC of sewage sludge (SS) and coconut shells, with $ZnCl_2$ as a catalyst, was investigated to evaluate its effectiveness in enhancing the co-HTC process. Response surface methodology was employed to optimize key parameters, including the raw material ratio, temperature and reaction time. The optimized parameters were subsequently applied to the co-HTC process. The raw materials and resulting hydrochars were characterized using proximate and ultimate analyses, higher heating value (HHV) determination, Fourier transform infrared spectroscopy and thermogravimetric analysis. The results revealed that the fuel ratio of raw SS increased significantly, from 0.09 in untreated SS to 0.26 in co-HTC, and further to 0.41 in $ZnCl_2$-aided co-HTC. The carbon content of the hydrochar increased, accompanied by a notable reduction in the H/C and O/C atomic ratios. The HHV improved substantially from 5.8 MJ/kg for raw SS to 11.1 MJ/kg in co-HTC and 14.0 MJ/kg in $ZnCl_2$-aided co-HTC. The combustion characteristic index demonstrated superior combustion performance for the $ZnCl_2$-aided co-HTC process, achieving a value of 33×10^{-7} min^{-2} $°C^{-3}$. Additionally, the synergistic effects on HHV were significantly enhanced, with the synergistic coefficient increasing from 0.79% in co-HTC to 27.00% in $ZnCl_2$-aided co-HTC. Overall, $ZnCl_2$ effectively catalyzes the co-HTC process, enabling the production of higher-quality solid fuels.

Keywords

hydrothermal co-carbonization, zinc chloride, sewage sludge, optimization, synergistic effect

1 Introduction

Sewage sludge (SS) is an inevitable waste product generated by municipal wastewater treatment facilities that are majorly composed of organic contaminants, microorganisms, heavy metals and abundant nutrients [1]. Currently, the most common approaches in disposing of sewage sludge are through landfilling, composting and incineration which presents limitations in terms of high energy consumption and environmental concerns [2]. However, the goal of sustainable development and circular economy is that wastewater should be considered primarily as a source of water, then energy, organics, metals and other resources. A favorable solution that can aid reduce waste volume and enhance energy recovery is by producing hydrochar from SS through hydrothermal carbonization (HTC) [3]. HTC is a thermochemical method that transforms biomass and organic waste to solid biofuel, liquid and gaseous products in the presence of water acting as the catalyst - at a subcritical state, water increases its ionization thus increasing the ionic reaction or hydrolysis. The common parameters that concern this process are temperature with a range of 150–300 °C and reaction time from a few minutes up to 48 h; the pressure used is typically autogenous [4]. Since water is important in the HTC process, SS which usually has a high moisture content that reaches up to 96.2% will be fitting as a feed for the process [4]. Consequently, Cavali et al. [5] conducted a study regarding the hydrothermal carbonization

Cite this article as: Arriola, M. J., Cantalejo, R. F., Perona, M. J. A., Policarpio, F., Rubi, R. V., Olay, J. "Hydrochar Derived from Zinc Chloride Aided Hydrothermal Co-carbonization of Sewage Sludge and Coconut Shells (*Cocos nucifera*)", Periodica Polytechnica Chemical Engineering, 2026. https://doi.org/10.3311/PPch.42388

of non-dewatered sewage sludge and ultimately promoted a more sustainable HTC process.

Notwithstanding the potential of HTC, some studies have indicated that the fuel and combustion characteristics of hydrochar from SS are dissatisfying [6]. This is because hydrochar properties are highly dependent on the type of raw material to be used, e.g., hydrochar from sewage sludge shows a relatively lower yield compared to lignocellulosic biomass which generally has a high yield [7]. Therefore, introducing lignocellulosic biomass with SS was explored to determine if it can improve the fuel quality of the hydrochar which is then called hydrothermal co-carbonization (co-HTC) [2]. Zhai et al. [3] investigated the hydrothermal co-carbonization between SS and sawdust, corncob, cornstalk and rape straw which all increased the higher heating value (HHV). Furthermore, co-HTC has also been investigated in the adsorption properties of a hydrochar from sewage sludge and coconut shells (CS) [1]. However, no results regarding fuel characteristics were presented in that study. Since coconut shells are a good biomass fuel and an excellent source of charcoal, they can be a relevant co-feed with SS to improve its HHV. Additionally, coconut shells are discarded or burnt unprocessed, resulting in poor sanitation and contamination of the environment. The concern is that the open burning and inappropriate disposal of coconut shells contribute to poor sanitation and air pollution. From this, utilizing coconut shells can contribute to lessening its environmental concern while potentially enhancing a hydrothermal process.

The organic composition of SS is composed of a mixture including protein, polysaccharides, inorganic materials and lipids. During the HTC process, proteins and polysaccharides are depolymerized and hydrolyzed to produce amino acids and monosaccharides respectively. These two products undergo a Maillard reaction to produce heterocyclic compounds which will then be polymerized to generate hydrochar. On the other hand, lignocellulosic biomass, coconut shells, are composed of cellulose, hemicellulose and lignin. The hemicellulose composition also undergoes depolymerization which results in a polysaccharide [8]. With that, in co-HTC, the interaction between protein and polysaccharide results in the formation of hydrochar which is influenced by the Maillard reaction. The synergistic effect between these two types of raw material is dependent on the strength of the Maillard reaction which is catalyzed in an acidic reaction [9]. Concerning catalysts, Abd Rahman et al. [10] explored the effects of zinc chloride loading in hydrothermal carbonization of cotton textile waste which increased its HHV. Typically, a subsequent activation is done as a further carbonization step increasing the aromatic content, the porosity and the stability of the hydrochars. Steam is used in physical activation tests; for chemical activation KOH, NaOH, $ZnCl_2$ or H_3PO_4 are used [11]. However, the conventional two-step methods for activation consume a lot of energy and thus, one-pot synthesis was studied and was found effective [12]. To date, as far as the best knowledge of the researchers, no studies have been conducted regarding the $ZnCl_2$-assisted hydrothermal co-carbonization specifically of sewage sludge with coconut shells for fuel characteristics.

In this study, the researchers used sewage sludge and coconut shells (*Cocos nucifera*) to produce hydrochars via zinc chloride-assisted co-HTC. The study aims to investigate the feasibility of $ZnCl_2$ as a catalyst in the hydrothermal co-carbonization process of SS and CS to obtain high quality solid fuel. Also, varying parameters were examined which were: sewage sludge to coconut ratio (1:0.3; 0:0.5; 1:0.7), temperature (180 °C; 200 °C; 220 °C) and residence time (1 h; 1.5 h; 2 h). These parameters and feedstock were fed in a Teflon-lined hydrothermal autoclave reactor to perform the hydrothermal co-carbonization process. The produced hydrochars were assessed by hydrochar yield (HY) along with its HHV. These were then analyzed and optimized through the response surface methodology – Box Behnken design (RSM-BBD) approach. Afterward, the optimized parameters were used in producing a hydrochar that were characterized along a hydrochar following the same parameters but without zinc chloride. The characterizations for the hydrochar were the proximate analysis, ultimate analysis, Fourier transform infrared spectroscopy (FTIR) and thermogravimetric analysis (TGA). Finally, the synergistic effect of the sewage sludge and coconut shells under the presence of zinc chloride were assessed based on the acquired results.

2 Materials and methods

2.1 Collection of raw materials

The SS used in the experiments, with 91.14% moisture, was obtained from a wastewater treatment facility in the Philippines and was stored at cool temperature. The CS used was obtained from a wet market across in Quiapo, Manila. Moreover, zinc chloride with 98% purity was purchased in DKL Laboratory supplies while concentrated

hydrochloric acid was purchased in the Chemistry Laboratory of Adamson University. All of the chemicals used were analytical reagent grade.

2.2 Raw material preparation

The gathered coconut shells were washed with distilled water, crushed into smaller chunks, and then dried at 105 °C in a convection oven until weight was slightly constant. Subsequently, the coconut shells were pulverized using laboratory mill and were sieved through 60-mesh (0.25 mm) using ro-tap sieve shaker. On the other hand, gathered sewage sludge was not dried and pulverize to promote sustainability [5].

2.3 $ZnCl_2$-aided hydrothermal co-carbonization

The hydrothermal carbonization experiments were conducted in a Teflon-lined hydrothermal autoclave reactor (Techinstro, Maharashtra, India). Firstly, 80 g of the SS is diluted with distilled water by 8:1 (m/v) sewage sludge to water ratio to provide effortless stirring and then mixed with $ZnCl_2$ at a solute to water ratio of 1:40 (m/v). The required amount of $ZnCl_2$ was referred to the findings of Rosly et al. [13] that explored the effects of $ZnCl_2$ loading in hydrothermal carbonization. The water pertaining to the amount of $ZnCl_2$ was the water in the sewage sludge plus the additional water for dilution. Following, the mixture was then fed in the 250 mL Teflon-liner along with the 30%–70% (m/m) pre-treated coconut shells to the dry basis of sewage sludge. The reactor was placed in a furnace which was heated to varying temperatures of 180 °C–220 °C. The timer started when the desired temperature was reached and the residence time was 1–2 h. All varying parameters were with the basis from previous literatures [14, 15] respectively.

At the end of the reaction, the reactor was cooled to room temperature and then, the hydrochar produced was soaked to HCl (10 m%) for 15 min to remove residual salt and consequently was vacuum filtered. The filtered hydrochar was further washed with distilled water. The washed hydrochar was dried through a convection oven until slightly constant weight at 105 °C. Finally, after cooling to room temperature, hydrochar was sealed in an airtight container until characterization and analysis. The hydrochars were labeled as HC-Ratio-Temp-Time-Catalyst, e.g., (HC-1:0.5-200 °C-1.5-W), where 1:0.5 represents dried basis sewage sludge to coconut shells ratio and was produced at 200 °C and 1.5 h with the presence of catalyst. The absence of $ZnCl_2$ will be presented with WO.

2.4 Design of experiment

The three factors investigated in this study—sewage sludge to coconut shell ratio, temperature and residence time—were selected because they are the primary variables known to influence hydrothermal carbonization performance, particularly HY and HHV. These parameters strongly affect biomass decomposition, hydrolysis, dehydration and carbonization pathways, as established in previous HTC studies. Other operational variables such as catalyst loading, water-to-biomass ratio, particle size, heating rate and initial moisture content can also influence HTC outcomes; however, these were held constant to isolate the effects of the three main factors and maintain experimental control. Only ratio, temperature and residence time were varied according to the Box–Behnken design, while all other parameters were fixed during the experiments. The ratio of coconut shells was assessed in the range of 0.3–0.7 in reference to the dried amount of sewage sludge. The temperature varies from 180–220 °C while time covers 1–2 h. Three inputs from these parameters were represented by numerical values where −1 was assigned for lower, 0 for average and +1 for higher (Table 1).

Response surface methodology was applied using a Box–Behnken design in Design-Expert v7 [16] and Minitab [17] to evaluate the effects of the selected factors on HY and HHV. In this context, RSM represents the overarching statistical approach used to model and optimize the process, while BBD serves as the specific experimental design framework that determines the number and distribution of experimental runs.

The BBD distributes experimental points evenly across the experimental domain by positioning runs at the midpoints of factor combinations while holding the third factor at its center level. This configuration avoids corner points and creates a balanced, symmetrical layout that effectively captures system curvature with fewer experiments. Because BBD does not require all possible factorial combinations, it substantially reduces the total number of experiments; for example, a full three-factor factorial design would require 27 runs, whereas the BBD used here required only 17.

Table 1 Input parameters and their code levels

Factors	Unit	Coded factor levels		
		−1	0	+1
Ratio	-	0.3	0.5	0.7
Temperature	°C	180	200	220
Time	h	1	1.5	2

Similar applications of RSM–BBD for optimizing hydrothermal conversion and biomass processing have been reported by Amenyeku et al. [18], Raheem et al. [19], Shakiba et al. [20] and Sulaiman et al. [15], further supporting the suitability of this design approach for the present study.

In this study, the design consisted of 17 experimental runs, including five center-point replicates to assess model reliability and experimental consistency. The completed dataset was analyzed using regression techniques to identify significant effects and develop the final predictive models for HY and HHV.

The significance of model terms (main effects, two-factor interactions and quadratic terms) was assessed by analysis of variance (ANOVA) using *F*-tests; *p*-values from ANOVA were used to identify statistically significant terms ($\alpha = 0.05$). Non-significant terms were removed during model reduction to produce the final reduced model. Model adequacy was then verified using R^2, adjusted R^2, predicted R^2 and diagnostic checks (residual analysis and lack-of-fit test) prior to interpretation and optimization.

2.5 Hydrochar characterization

Hydrochars produced from the runs in the design experiment were characterized by HY and HHV only for optimization. Further characterization was applied to hydrochars derived from the optimized parameters. These hydrochars include the co-HTC with $ZnCl_2$, co-HTC without the $ZnCl_2$, the HTC of SS and the HTC of CS.

2.5.1 Hydrochar yield and higher heating value

The HY determines how much hydrochar is produced from the hydrothermal carbonization. It is determined by the mass of hydrochar obtained divided by the mass of the feedstock used. The HY was calculated using the Eq. (1):

$$\text{HY}\% = \frac{\text{Mass of hydrochar}}{\text{Initial mass of feedstock}} \times 100 \,. \quad (1)$$

Subsequently, the HHV of the hydrochars were obtained by a microprocessor bomb calorimeter. This test would determine the amount of energy that can be obtained within the hydrochar and its potential as an alternative fuel.

2.5.2 Proximate and ultimate analysis

The ash (ASH) and volatile matter (VM) content of hydrochars, for proximate analysis, was determined using the methods of ASTM D1762-84(2021) [21] while fixed carbon (FC) was determined using the methods of ASTM D3172-13(2021)e1 [22]. The ultimate analysis of the hydrochars, which includes the C, H and O, were calculated using empirical model correlations based on the proximate analysis. The calculations follow Eqs. (2)–(4) respectively:

$$\text{C} = -35.9972 + 0.7698\text{VM} + 1.3269\text{FC} + 0.3250\text{ASH} \quad (2)$$

$$\text{H} = 55.3678 - 0.4830\text{VM} - 0.5319\text{FC} - 0.5600\text{ASH} \quad (3)$$

$$\text{O} = 223.6805 - 1.7226\text{VM} - 2.2296\text{FC} - 2.2463\text{ASH} \,. \quad (4)$$

These correlations are applicable in a larger range of proximate and ultimate analysis unlike those of other linear models. The mean absolute errors (MAE) of these models are 2.58%, 0.41%, 2.60% and the average biased error (ABE) are 0.45%, 2.82%, 2.01% for carbon, hydrogen and oxygen respectively.

2.5.3 Fourier transform infrared spectroscopy

The FTIR (Shimadzu, Kyoto, Japan) analytical method was used to describe the surface functional groups found in a compound with a wavenumber range of 4000–500 cm^{-1}.

2.5.4 Thermogravimetric analysis

The TGA (LECO Corporation, Michigan, USA) analytical method was used to study the burning characteristics of raw materials and the hydrochars. The inlet air gas flow rate was 50 mL/min and the heating rate was 20 °C/min with the combustion interval set from 50 °C to 800 °C. The fuel performance of the samples was further investigated using the composite combustion index (CCI, 10^{-6} min^{-2} $°C^{-3}$) as shown by Eq. (5).

$$\text{CCI} = \frac{R_m \times R_a}{T_i^2 \times T_b} \quad (5)$$

Where R_m (% min^{-1}) indicates the maximum rate of weight loss, R_a (% min^{-1}) shows the average rate of weight loss, T_i (°C) represents the ignition temperature and T_b (°C) denotes the burnout temperature. The temperature where the fuel begins to burn is the ignition temperature, the derivative thermogravimetry (DTG) peak temperature is maximum combustion rate temperature (T_m), while the temperature where the percent mass loss rate is less than 1 m% min^{-1} is the burnout temperature [2].

2.5.5 Synergistic effect

The synergistic coefficient (SC) quantifies the synergistic or anti-synergistic effects of the two feedstocks. This will be evaluated by the HY and HHV following Eq. (6).

$$SC = \frac{\text{experimental value} - \text{calculated value}}{\text{calculated value}} \times 100 \quad (6)$$

Calculated value is the theoretical value that can be obtained given the different fractions. For example, when SS and CS were mixed with a mass ratio of 1:0.5, the calculated value of the HY (CHY) was calculated as Eq. (7).

$$\text{CHY}(\%) = \frac{1}{1.5}\eta_{SS} + \frac{0.5}{1.5}\eta_{CS} \quad (7)$$

Where η_{SS} and η_{CS} are the HY of SS and CS, respectively [23].

3 Results and discussion

3.1 Process parameter effects on hydrochar production

3.1.1 Statistical modeling of hydrochar yield

The effects of different process parameters on HY and HHV were evaluated using the Box Behnken design. The quadratic model was selected based on the results of the BBD and the statistical analysis performed using Design-Expert v7 [16]. The model demonstrated high R^2, adjusted R^2 and predicted R^2 values, indicating that it effectively captures the variability in HY and HHV within the experimental range. Significant terms identified by ANOVA ($p < 0.05$) further support the relevance of the selected factors and their interactions. Although residual analysis was not explicitly reported in the manuscript, the software's internal checks for model adequacy and aliasing, combined with the balanced experimental design, suggest that the model provides a reliable representation of the system. Therefore, the predictions and optimizations reported are considered valid within the experimental factor space, while acknowledging that extrapolation beyond this range should be approached with caution. Table 2 shows the results obtained from the experimental design. Through these responses, Design-Expert v7 [16] software was able to analyze the results and plot the different relationship among the parameters and their effect on the HY and HHV of the hydrochars. To proceed with the optimization, the responses and variables were initially fitted to different models and analyzed on the type of equation will fit the most. The "Std" column represents the standard order of the Box–Behnken design generated by Design-Expert [16], while the "Run" column indicates the randomized order in which the experiments were carried out. Randomization is applied to reduce systematic bias and ensure the validity of the statistical analysis. Table 3 shows the different equation model that can be utilized to predict and optimize the results obtained from the experiment. The model evaluation (Table 3), it is essential to summarize the model parameters. The quadratic model incorporates three independent variables: A (sludge-to-coconut shell ratio), B (temperature) and C (residence time). The model accounts for main effects (A, B, C), two-way interactions (AB, AC, BC) and

Table 2 Obtained response for hydrochar yield and higher heating value from hydrochar production

Std	Run	Factor 1: Ratio of coconut shell	Factor 2: Temperature	Factor 3: Time	Response 1: Hydrochar yield	Response 2: HHV
-	-	-	°C	h	%	MJ/kg
14	1	0.5	200	1.5	50.9	14.11
5	2	0.3	200	1	44.82	13.48
15	3	0.5	200	1.5	50.9	14.11
1	4	0.3	180	1.5	46.74	12.82
11	5	0.5	180	2	48.5	14.15
2	6	0.7	180	1.5	60.14	13.68
7	7	0.3	200	2	44.85	12.88
17	8	0.5	200	1.5	50.9	14.11
8	9	0.7	200	2	49.07	13.7
6	10	0.7	200	1	47.36	14.1
4	11	0.7	220	1.5	56.3	13.65
3	12	0.3	220	1.5	41.11	13.61
13	13	0.5	200	1.5	50.9	14.11
10	14	0.5	220	1	43.7	14.15
12	15	0.5	220	2	34.19	12.45
16	16	0.5	200	1.5	50.9	14.11
9	17	0.5	180	1	42.22	13.58

Table 3 Model summary statistics*

Source	R^2		Adjusted R^2		Predicted R^2		Remarks
	HY	HHV	HY	HHV	HY	HHV	
Linear	0.3826	0.2827	0.2401	0.1171	0.2140	0.3157	
2FI	0.4943	0.6094	0.1909	0.3750	1.2725	0.2343	
Quadratic	0.8879	0.8919	0.7437	0.7530	0.7938	0.7293	Suggested for both
Cubic	1.0000	1.0000	1.0000	1.0000			Aliased for both

* R^2: regression coefficient

quadratic terms (A^2, B^2, C^2) to capture potential nonlinear effects among the factors. Table 3 presents the statistical indicators (R^2, adjusted R^2, predicted R^2) for each model type considered. Although the cubic model shows an R^2 of 1, it is aliased and cannot reliably estimate all effects with the given experimental matrix. Therefore, the quadratic model was selected based on its high fit, predictive ability and non-aliased nature, providing a reliable basis for subsequent optimization of HY and HHV.

The different models of which the obtained results are incorporated into are linear, two-factor interaction (2FI), quadratic and cubic equations. To evaluate which model can depict more accuracy, R^2 (regression coefficient), adjusted R^2 and predicted R^2 are taken into consideration [18]. A higher value for these mentioned coefficients shows a more desirable model since R^2 describes how well the model fits the data; adjusted R^2 modifies the number of terms in the model for more reliable measure of fit. On the other hand, predicted R^2 is the predictive ability of the regression model for unseen data. From this, a quadratic model is chosen as the model and that has been suggested for both the HY and HHV responses because of its higher value. Despite having a value of 1 for cubic model, it is not chosen as its model since it is remarked as aliased for the responses, signifying that the experimental design is not possible to estimate all effects using this matrix since it has fewer unique combinations than a full-factorial design.

Following the quadratic model for data fitting, Table 4 presents the *p*-value from analysis of variance (ANOVA) for determining the significance of the independent variables (A-Ration; B-Temperature; C-Time) and their relationship with the dependent variables namely HY and HHV.

In the ANOVA analysis, *p*-values indicate the probability of observing the experimental data assuming that the corresponding term has no effect on the response variable (null hypothesis). Terms with *p*-values less than 0.05 were considered statistically significant, suggesting that these factors or their interactions have a meaningful influence on HY or HHV. Terms with *p*-values greater than 0.05 were considered non-significant and could be excluded during model refinement. This interpretation, combined with the high R^2, adjusted R^2 and predicted R^2 values, supports the reliability of the quadratic model within the studied experimental range [19]. From the results presented in Table 5, the significant terms for HY are A, B, BC and C^2 while the significant terms for HHV are A, C, BC, A^2 and B^2, since these terms showed a *p*-value less than 0.05. On the other hand, C, AB, AC, A^2 and B^2 are terms

Table 4 Estimated effects and 95% confidence intervals for hydrochar yield and higher heating value models

	HY			HHV		
Term	Coef[a]	SE Coef[b]	95% CI[c]	Coef[a]	SE Coef[b]	95% CI[c]
Constant	−291	159	(−667, 84)	−42.7	13.8	(−75.3, −10.0)
Ratio	−63.4	87.3	(−269.8, 143.1)	19.87	7.60	(1.91, 37.83)
Temp.	2.50	1.50	(−1.06, 6.05)	0.422	0.131	(0.113, 0.732)
Time	156.2	35.9	(71.3, 241.2)	13.13	3.13	(5.74, 20.52)
Ratio × Ratio	56.8	36.9	(−30.3, 144.0)	−8.91	3.21	(−16.49, −1.32)
Temp. × Temp.	−0.00525	0.00369	(−0.01397, 0.00347)	−0.000784	0.000321	(−0.001543, −0.000026)
Time × Time	−26.59	5.90	(−40.54, −12.64)	−0.855	0.513	(−2.068, 0.358)
Ratio × Temp.	0.112	0.378	(−0.782, 1.006)	−0.0512	0.0329	(−0.1291, 0.0266)
Ratio × Time	4.2	15.1	(−31.6, 40.0)	0.50	1.32	(−2.61, 3.61)
Temp. × Time	−0.395	0.151	(−0.752, −0.037)	−0.0568	0.0132	(−0.0879, −0.0256)

[a] Coef = Estimated regression coefficient
[b] SE Coef = Standard error of the coefficient
[c] 95% CI = 95% confidence interval

Table 5 The *p*-value results from ANOVA for response surface quadratic model

Source	*p*-value	
	HY	HHV
Model	0.0128	0.0114
A-Ratio	0.0044	0.0163
B-Temperature	0.0351	0.6345
C-Time	0.8667	0.0243
AB	0.7759	0.1633
AC	0.7893	0.7153
BC	0.0349	0.0035
A^2	0.1671	0.0274
B^2	0.1974	0.0444
C^2	0.0028	0.1396

deemed insignificant for HY whereas terms B, AB, AC and C^2 are not significant for HHV because of the *p*-value greater than 0.05. Table 5 presents the *p*-values from ANOVA for the independent variables affecting hydrochar yield and HHV. While these *p*-values indicate which terms are statistically significant ($p < 0.05$), Table 5 does not include mean squares, *F*-values, or estimated effects, providing limited insight into the relative contributions of each term or the need for model reduction. A more comprehensive table including these statistics would allow for a clearer understanding of the magnitude and direction of each effect, as well as the adequacy of the quadratic model. Nevertheless, the combination of significant *p*-values and high R^2, adjusted R^2 and predicted R^2 values supports the reliability of the model within the experimental range, and the conclusions regarding factor significance and optimization remain valid for the studied conditions.

Uncertainty of estimated parameters

In response surface methodology, the uncertainty of estimated parameters is typically evaluated through the standard errors of regression coefficients, confidence intervals and diagnostic measures that assess model stability and predictive reliability. The uncertainty and precision of the estimated parameters were evaluated through the standard errors and 95% confidence intervals (Table 4). These metrics quantify the margin of error for each factors effect, ensuring the reliability of the predictive models.

First, the adequacy of each model was confirmed using ANOVA-based significance testing, which evaluates the relative contribution of each term while accounting for experimental variability. The high coefficients of determination (R^2 and adjusted R^2) and the agreement between predicted and actual values indicate that the parameter estimates are stable within the range of the experimental design. In addition, the non-significant lack-of-fit results suggest that the residual variance of the models is consistent with the inherent variability of the experimental system, further supporting the reliability of the estimated parameters.

Second, the Box–Behnken design inherently incorporates model uncertainty through its structured distribution of experimental points, which provides balanced estimation of linear, quadratic and interaction terms. The presence of replicated center points also contributes to uncertainty estimation by allowing the separation of pure error from lack-of-fit. Because these replications showed minimal variability, the resulting model parameters can be interpreted as having relatively low experimental uncertainty.

Finally, the model predictions were compared with the experimental observations across the experimental factor space and the close agreement between the two provides additional support for the robustness of the estimated parameters despite the absence of explicit numerical confidence intervals. While detailed parameter-level uncertainty metrics could not be reported, the combination of design-based controls, model adequacy measures and experimental replication provides a comprehensive basis for assessing the reliability of the parameter estimates in this study.

Model assumptions and validation

Response surface methodology using the BBD relies on several standard assumptions, including the normality of residuals, independence of errors and constant variance across experimental runs. Although the detailed residual plots and diagnostic statistics from Design-Expert v7 [16] were not retained, the softwares internal validation checks, including ANOVA-based significance testing, lack-of-fit analysis and replication of center points, provide indirect verification that these assumptions were reasonably satisfied. The non-significant lack-of-fit results indicate that the model residuals are consistent with the inherent variability of the experimental system. In addition, the high coefficients of determination (R^2, adjusted R^2, predicted R^2) and agreement between predicted and observed values support the adequacy of the quadratic models. Collectively, these measures provide assurance that the assumptions underlying the fitted models are not violated, and the conclusions drawn from the models are reliable within the experimental factor space. Verification of mathematical assumptions was performed using the residual plots in Figs. 1 and 2. The normal probability plots show residuals

following a linear distribution, confirming normality. The "Versus Fits" plots show no discernable patterns, confirming homoscedasticity (constant variance). Finally, the "Versus Order" plots confirm the independence of the observations. By satisfying these assumptions, the model is confirmed as a valid mathematical representation of the process, rather than a mere statistical fit (R^2).

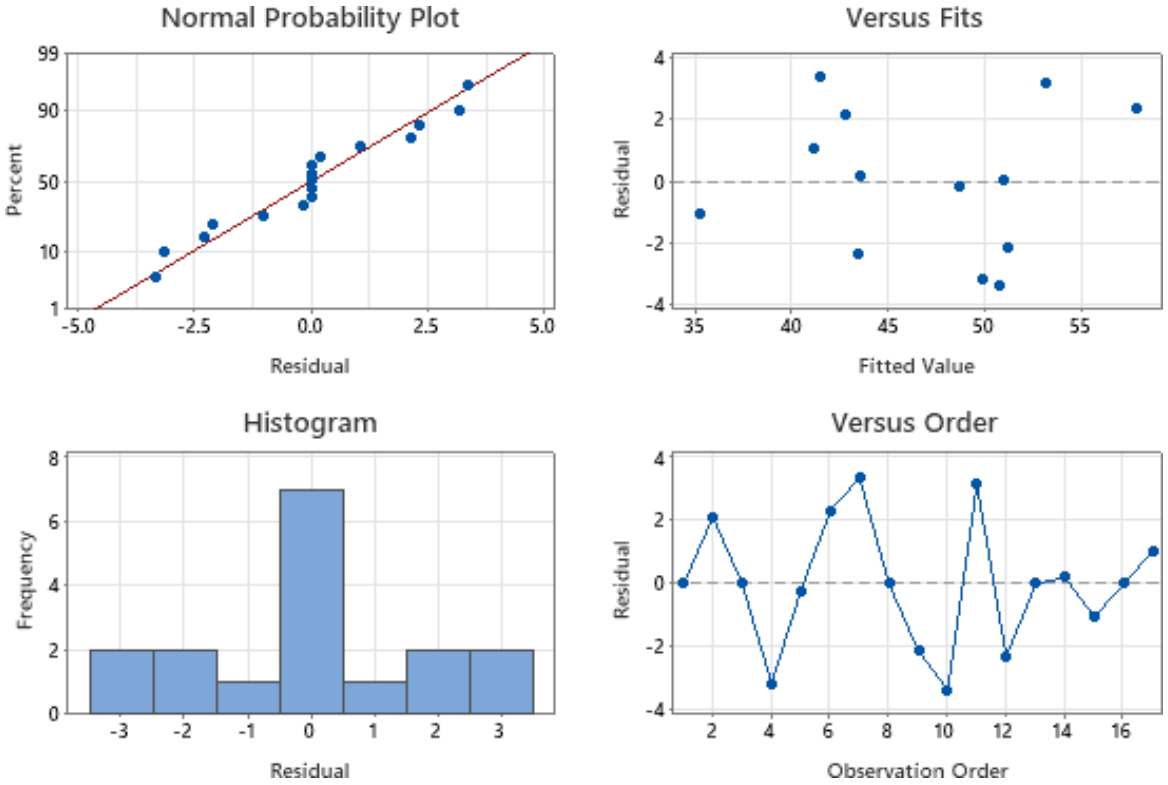

Fig. 1 Residual plot for hydrochar yield

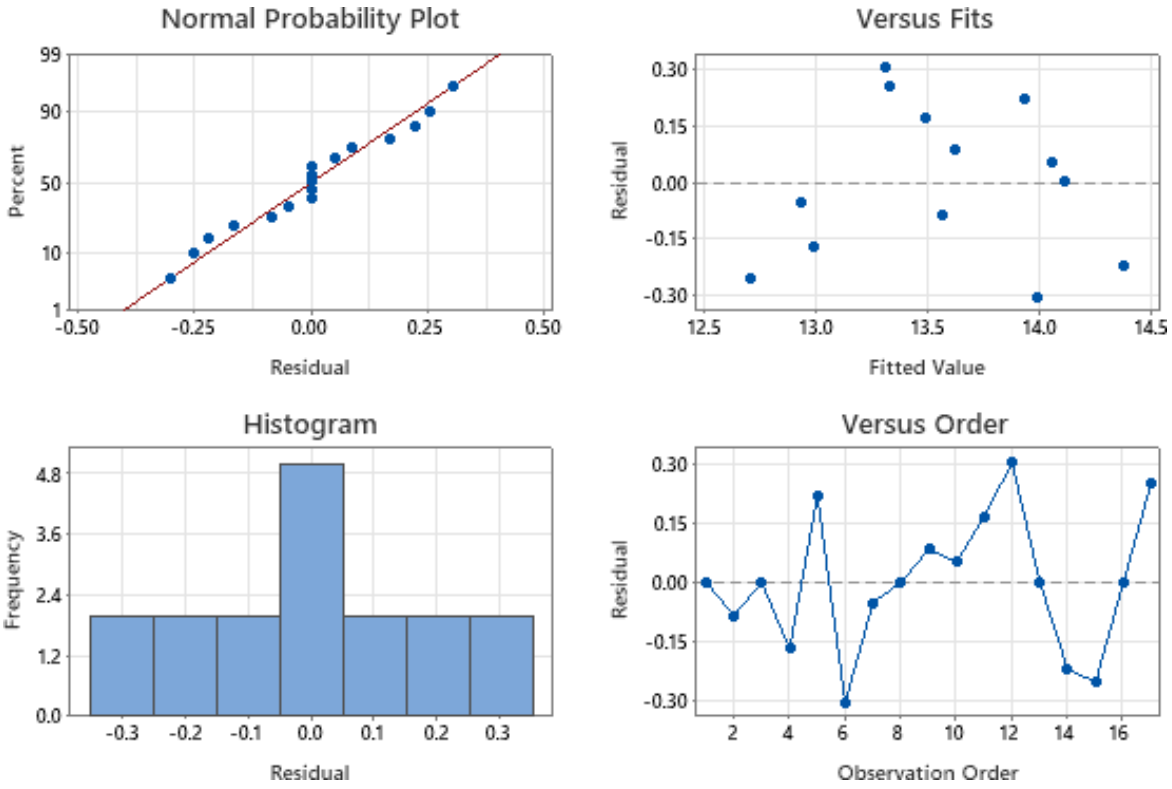

Fig. 2 Residual plot for higher heating value

Model evaluation considerations

While the ANOVA results presented in Table 5 show the *p*-values for all main and interaction terms, the detailed numerical outputs, including mean squares and *F*-values, were utilized to evaluate the relative contributions of each term. The high *F*-values associated with the significant terms ($p < 0.05$) further support the adequacy of the quadratic models. Although these additional statistics could provide further insight into the relative contributions of each term, the combination of *p*-values, high coefficients of determination (R^2, adjusted R^2 and predicted R^2), non-significant lack-of-fit and agreement between predicted and observed responses provide sufficient evidence that the quadratic models reliably describe the system within the experimental factor space.

Similarly, graphical effect plots, which are commonly used to visually interpret main and interaction effects, could not be reproduced due to the unavailability of the raw software outputs. To aid interpretability, Figs. 3 and 4 qualitatively illustrate the trends and interactions among process parameters, providing conceptual insight into the influence of temperature, residence time and feedstock ratio on HY and HHV. Such visualizations allow the reader to understand factor effects and interactions even without numerical effect plots and are consistent with standard practice when raw outputs are unavailable [24, 25].

Collectively, these considerations acknowledge the limitations of the reported outputs while supporting the reliability and interpretability of the fitted quadratic models.

3.1.2 Descriptive interpretation of process parameters

Section 3.1.2 provides a qualitative interpretation of how temperature, residence time and feedstock ratio influence hydrochar formation during hydrothermal carbonization. The discussion presented here is not derived from statistical modeling and is not used for predictive or inferential purposes. Instead, it offers a conceptual description based on general HTC reaction mechanisms reported in the literature and on observed experimental tendencies in this study. The statistically validated results and optimization outcomes remain those presented in Section 3.1.1.

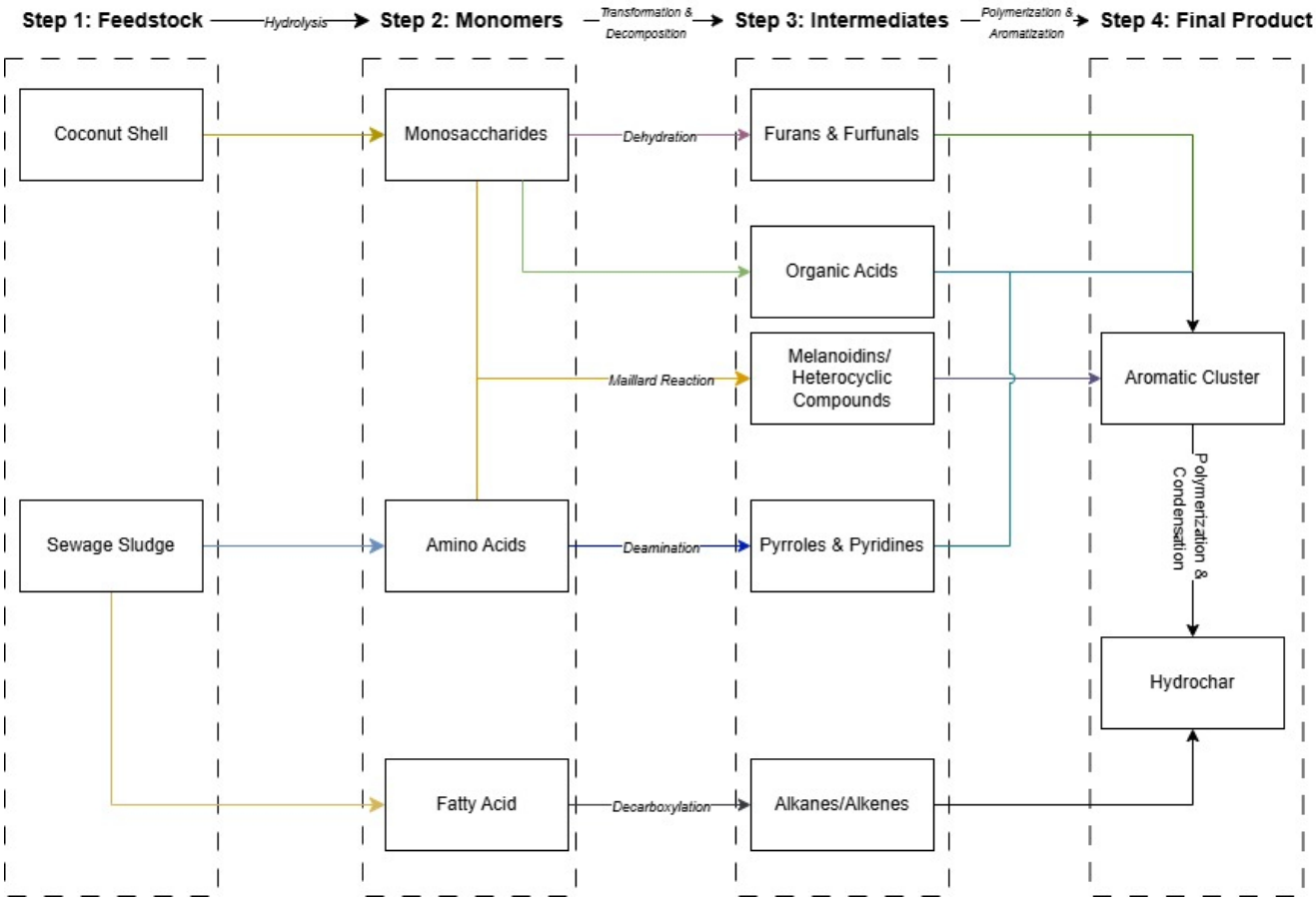

Fig. 3 Hydrothermal co-carbonization pathways and mechanism of sewage sludge and coconut shell

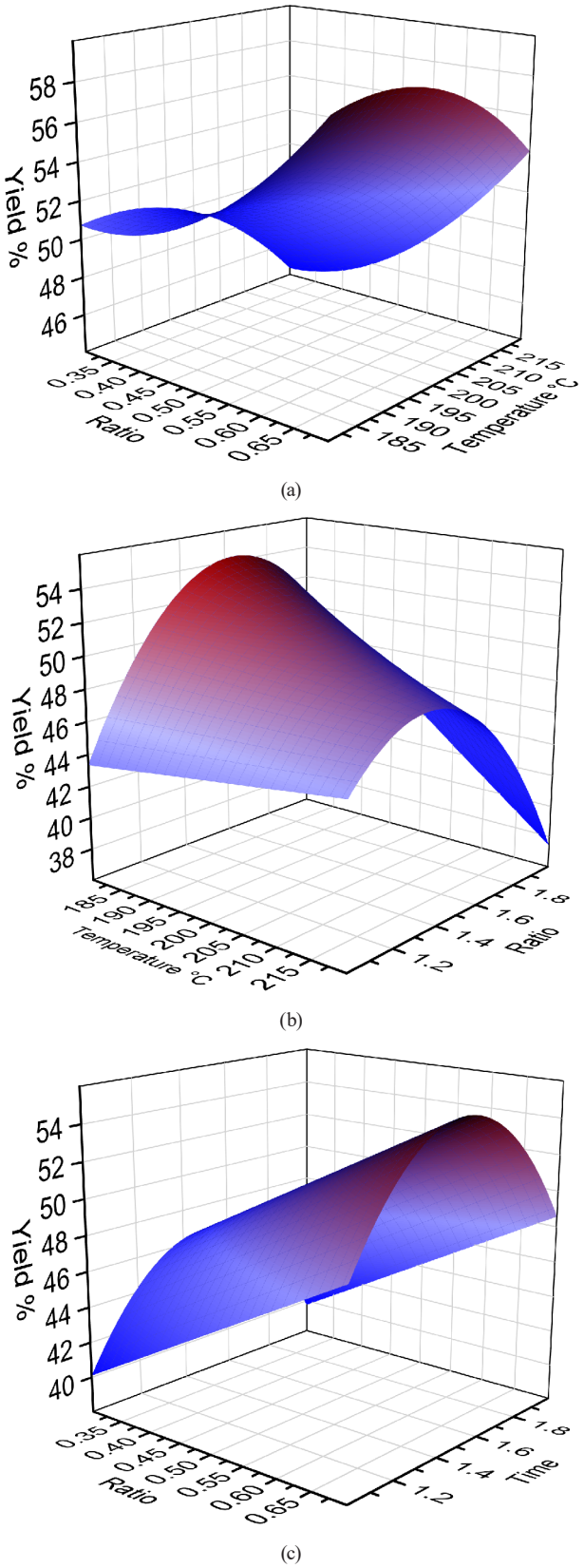

Fig. 4 Three-dimensional surface plot of the hydrochar yield response on the influence of (a) ratio and temperature with a hold value time of 1.5, (b) ratio and time with a hold value temperature of 200 °C, (c) temperature and time with a hold value ratio of 0.5

Influence of temperature

Temperature is one of the primary drivers of HTC chemistry. Increasing temperature accelerates dehydration, decarboxylation and aromatization reactions that progressively transform raw biomass into carbon-rich hydrochar [24, 25]. At lower temperatures, biomass degradation is limited, often resulting in higher solid yields because fewer soluble intermediates are released into the liquid phase. As temperature rises, the breakdown of hemicellulose and cellulose intensifies, promoting the formation of more condensed aromatic structures while typically reducing solid mass recovery [26]. These well-established thermal behaviors are consistent with the tendencies observed in the present study.

Influence of residence time

Residence time influences the degree to which hydrothermal reactions proceed. Short reaction times generally restrict biomass decomposition, preserving a higher proportion of the initial solid material. As reaction time increases, dehydration and polymerization reactions continue, favoring the formation of more stable, carbon-rich structures [27]. Prolonged residence, however, may lead to secondary degradation or dissolution of intermediates, which can reduce overall HY [28]. These typical HTC patterns were reflected conceptually in the trends observed during experimentation.

Influence of feedstock ratio

Blending sewage sludge with coconut shell influences both the reaction environment and hydrochar characteristics. Coconut shell, being lignocellulosic, supplies higher fixed carbon and contributes to aromatic precursor formation [29]. In contrast, sewage sludge contains proteins, lipids and inorganic minerals that can modify reaction pathways and influence ash content or catalytic behavior during HTC [30]. Accordingly, varying the sludge-to-coconut shell ratio alters the chemical balance within the reactor and the experimental trends observed in this study align with these known distinctions between lignocellulosic and sludge-derived feedstocks

General remarks on process trends

Figs. 3 and 4 are included solely as conceptual illustrations of the qualitative tendencies described above. They do not represent regression-based predictions or statistical models and are not used for optimization or hypothesis

testing. Their purpose is to guide the reader in visualizing how general variations in process conditions may influence hydrochar formation mechanisms. All quantitative and inferential results remain confined to the validated RSM–BBD analysis presented previously.

3.1.3 Effects of process parameters on the higher heating value of hydrochar

The HHV of a biofuel characterizes the thermal conversion of the product. It is the heat released from the total combustion of the biofuel. Also, HHV depicts how much energy can be obtained from the biofuel/biomass and its potential to be used. Fig. 5 shows the different relationship of the parameters ratio, temperature and time to the HHV of the hydrochar.

The different significance of these parameters is presented in Table 4 and it shows that for each independent parameter, only ratio and time are considered significant. Hydrothermal carbonization of sewage sludge alone increases its HHV from its initial value however, the increase is still insufficient to be utilized as fuel due to high content of ash. Introducing a lignocellulosic biomass will improve its HHV due to its possible synergistic effect with the sewage sludge [2]. As shown in Fig. 5, the HHV of the hydrochar increases as the ratio increases. Its increase mechanism is similar with HY which is highly influenced by the Maillard reactions. This includes the formation of heterocyclic compounds from a series of reactions of depolymerization, decomposition (hydrolysis, dehydration, decarboxylation and deamination) and then the Maillard reaction. The formation of these fragments resulted in the increased experimental values of HY and HHV [7].

In contrast with the HY, the time parameter is deemed significant for HHV while temperature is not significant. Time was considered not significant for HY since the presence of zinc chloride, an acidic salt, reduces the activation energy and reduces the time required for the process to occur. However, for HHV, it is significant possibly because the combustible materials of the hydrochar is transformed and combusted into ash as time progressed, which is the reason why the changes in yield are not significant, but the HHV decreases as time progresses. Relating to that, Zhao et al. [7] had similar results wherein the HHV is relatively higher at shorter residence time and Merzari et al. [31] found that as time of the process increases, ash content increases. Subsequently, temperature is significant for HY since at higher temperatures, the yield decreases due to increase in decarboxylation, dehydration and conversion of volatile matter. Conversely, no significant changes will occur for HHV despite changes in temperature since the process is catalyzed, all conversions of the raw material component occurred into the energy emitting elements.

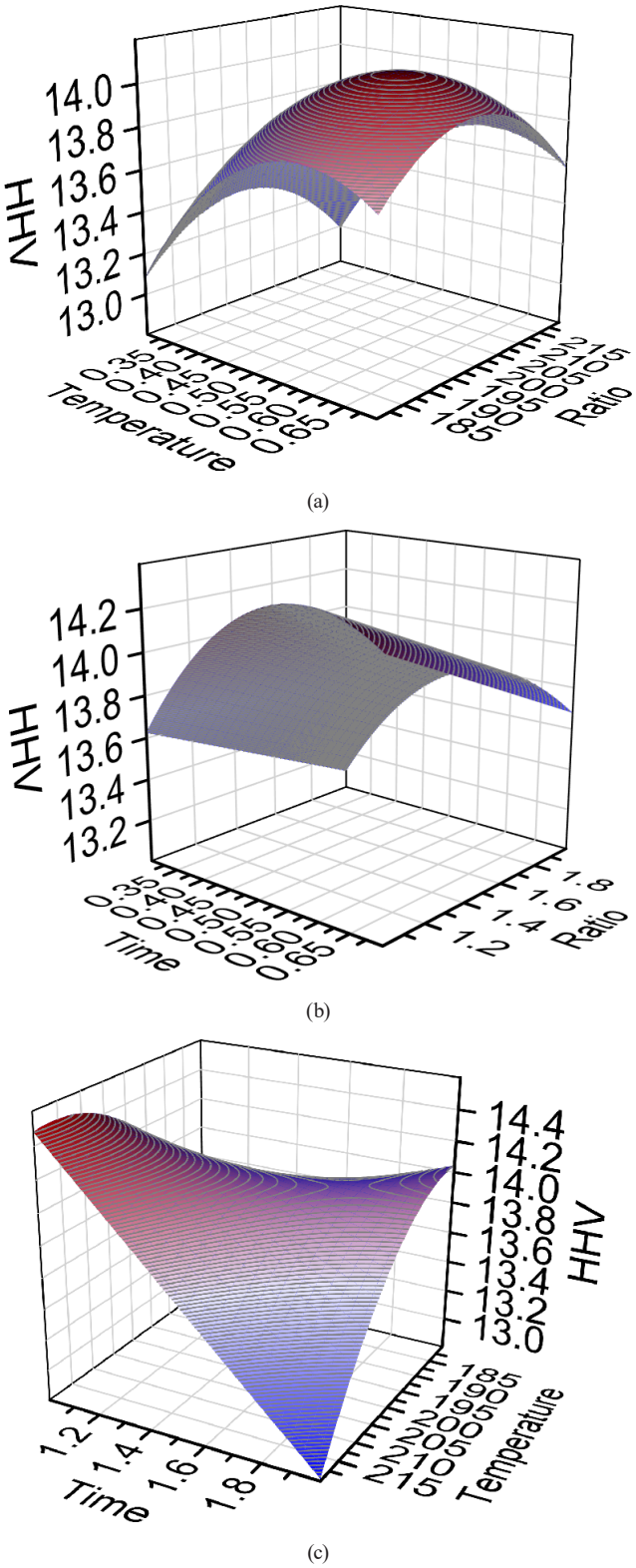

Fig. 5 Three-dimensional surface plot of the HHV response on the influence of (a) ratio and temperature with a hold value time of 1.5, (b) ratio and time with a hold value temperature of 200 °C, (c) temperature and time with a hold value ratio of 0.5

From the typical depolymerization of hemicellulose and protein at 180 °C while 210 °C for lignin and cellulose [9], zinc chloride in a solution can lower the temperature for decomposition of these components [12]. Also, Sulaiman et al. [15] had similar results where the temperature is not significant in increasing/decreasing the calorific value of the HHV. Overall, since temperature increases, some materials are lost thus the lowering of HY, but the identity of the hydrochar that contributes to its heat release is the almost the same thus, the insignificant change in HHV.

Similarly, with HY in terms of the interaction effects of the parameters, only the interaction between temperature and time has significant changes with HHV. This is because the ratio parameter has strong effects on the HHV of the hydrochar as shown in Fig. 5 (a), (b) wherein as the ratio increases, the HHV increases so much that changes of time and temperature are rather seen as not significant. In a study conducted by Multhaupt et al. [11] where zinc chloride was used as an assistant for hydrothermal carbonization of a lignocellulosic biomass, it was mentioned that $ZnCl_2$ helps break hemicellulose and cellulose structures in the biomass at significantly lower temperatures. With this, cellulose and lignin that are supposed to decompose at higher temperatures are now then broken down at lower temperatures thus, having insignificant difference in HHV between 180 °C and 220 °C. This also goes the same way for time since decomposition that is supposed to occur at longer hours is met at earlier time. Lastly, as shown in Fig. 5 (c), increasing the temperature or the time will result in an increase in HHV. Similar results were found with Raheem et al. [19] where the interaction effects of time and temperature

presented an increase in HHV with increase on the two parameters. At higher temperature, dehydration of the feedstock is increased resulting in an increase in carbon content and longer time ensures it meets its maximum level [32]. However, too much increase in temperature while time is also increased, will result in a decrease in HHV. This is because the presence of $ZnCl_2$ lowers the activation energy which results in gas evolution via decarboxylation and volatilization of organic contents thereby losing the fraction of carbon for both the solid and liquid phases [33].

3.1.4 Test optimization

According to Design-Expert v7 [16], model reduction may be applied by removing the model terms that are not significant, without counting that required to support hierarchy, to improve the model and optimization. Following this, model terms removed for HY are AB (RT), AC (Rt), A^2 (R^2) and B^2 (T^2), where R is the fuel ratio, T is the operating temperature and t is the operating time. Then this results in a HY estimation via quadratic regression model of

$$\begin{aligned}\mathrm{HY} &= -109.80271 + 22.09375R + 0.45275T \\ &+ 158.2325t - 0.39475Tt - 26.55167t^2.\end{aligned} \tag{8}$$

On the other hand, the model terms removed for HHV are AB (RT), AC (Rt) and C^2 (t^2). Then this results in a HHV estimation via quadratic regression model of

$$\begin{aligned}\mathrm{HHV} &= -37.27188R + 0.40781T + 10.8175t \\ &- 0.05675Tt - 9.1875R^2 - 0.0008125T^2.\end{aligned} \tag{9}$$

In optimization, the software has the option to adjust the goals for the parameters and responses. For this study, the parameters ratio, temperature and time are set into in range while both HHV and HY are set to maximize. This gave a solution wherein the optimal parameters are 0.66 ratio, 180 °C temperature and 1.82 h which will result in 56.97% HY and 13.93 MJ/kg HHV with a desirability of 0.86. These optimized parameters were used to produce hydrochars that were characterized. Similar process was conducted but hydrochar from $ZnCl_2$-aided hydrothermal co-carbonization was termed as the independent variable; which was compared with hydrochar derived from hydrothermal co-carbonization of sewage sludge and coconut shells, hydrochar derived from sewage sludge alone and coconut shells alone.

3.2 Characterization of raw materials and optimized hydrochars

After the optimization, the raw materials were characterized along with the hydrochars derived from the hydrothermal process parameters of temperature: 180 °C, time: 1.82 h and a ratio of 0.66 for the co-HTC process. Table 6 shows the different physicochemical properties of the raw materials and the derived hydrochars. The HY of SS and CS were 71.78% and 40.78% respectively and their HHVs are 9.12 and 13.85 respectively. Despite both raw materials having an increase in HHV once undergone hydrothermal carbonization, high HY and low HHV value are observed for HC-SS which corresponds to Zhao et al. [7] where hydrochar properties are highly dependent on the feedstocks. Moreover, the hydrothermal co-carbonization of SS with CS resulted in an increase on HY and HHV in relation to the hydrothermal carbonization of SS and CS alone signifying the effectiveness of co-HTC. Lastly, a decrease in HY was observed in the addition of $ZnCl_2$ but an increase on its HHV.

HY refers to the amount of hydrochar produced from a biomass sample during hydrothermal carbonization (HTC). The HC-SS sample has the highest yield at 71.78%,

Table 6 Proximate analysis, fuel ratio, ultimate analysis, atomic ratio, hydrochar yield and higher heating value

Sample	Proximate Analysis			Fuel Ratio (FC/VM)	Ultimate Analysis			H/C	O/C	HC Yield (%)	HHV (MJ/kg)
	FC (%)	VM (%)	Ash (%)		C (%)	H (%)	O (%)				
SS-Raw	4.10	44.16	51.74	0.09	20.25	2.88	22.25	1.71	0.82	-	5.79
CS-Raw	15.35	61.28	23.37	0.25	39.14	4.52	31.40	1.39	0.60	-	12.94
HC-SS	10.68	47.84	41.48	0.22	28.48	3.35	24.28	1.41	0.64	71.78	9.12
HC-CS	21.47	58.96	19.57	0.36	44.24	4.51	30.29	1.22	0.51	40.78	13.85
HC-SS&CS	11.84	45.21	42.95	0.26	28.47	3.18	22.92	1.34	0.60	62.17	11.09
HC-SS&CS&$ZnCl_2$	21.30	52.38	26.32	0.41	41.14	4.00	26.84	1.17	0.49	59.09	13.97

surpassing other samples. The high yield was mainly due to the high inorganic content of the SS while, the lower yield from CS corresponds to the lignocellulosic characteristic of the raw material [23]. The HHV quantifies the energy content of fuel samples, reflecting the total heat released when a unit mass of the fuel is completely combusted. A higher HHV indicates greater energy content in the sample. Among the tested samples, the co-HTC sample (HC-SS&CS&$ZnCl_2$) has the highest HHV at 13.97, signifying its superior energy potential compared to the other samples. This suggests that co-processing with zinc chloride enhances the energy characteristics of the fuel, making it more efficient for combustion applications.

3.2.1 Proximate analysis

From Table 6, the VM of hydrochar produced from CS decreased, while its FC increased in comparison to the raw CS. This devolatilization, decrease in VM, is due to the dehydration and decarboxylation reactions which consequently increase the FC corresponding to the aromatization and polymerization of the degraded products [5]. However, not all VM are transformed into FC as per the mass balance, the HY, denoting that some VM may be converted to liquid or gases [2]. The ash content of CS found similar results with Vargas-Delgadillo et al. [34] which was relatively high. Notwithstanding, the hydrothermal carbonization of both CS and SS resulted in a decrease in ash. This may possibly be because the inorganic content of the raw material is composed of potassium, reducing the ash content after HTC. Similar results with Wang et al. [8, 9] were observed in terms of the decrease in ash content from the raw material after hydrothermal carbonization process.

For co-HTC, an increase in ash content was observed because the added lignocellulosic biomass, CS, has relatively high ash content. Also, an increase in FC and a decrease in VM occurred which can be explained similarly with the hydrothermal carbonization of CS. Finally, a further decrease in the ash content was noticed with the addition of $ZnCl_2$ and correspondingly increased the FC and VM. The decrease in ash content is caused by the washing with HCl process prior to the vacuum filtration. The inorganic fraction, such as minerals and salts, is released from the carbon after acid-washing [12]. Additionally, the increase in its HHV was because of the aid of $ZnCl_2$, enhancing the dehydration, aromatization and decarboxylation reactions [10]. To assess the coalification degree of the hydrochar, or its suitability as a solid fuel, the fuel ratio was determined [23]. As shown in Table 6, the fuel ratio of the SS increased from 0.09 to 0.41 by undergoing $ZnCl_2$-aided hydrothermal co-carbonization. A higher fuel ratio signifies a better combustion performance [5].

3.2.2 Ultimate analysis

Table 6 provides the ultimate analysis, specifically elements which can be used to understand various applications, including fuel selection and combustion efficiency improvement. Carbon content in the samples varies significantly, ranging from 20.25% to 44.24% wherein higher carbon levels indicate greater potential for energy generation, as carbon contributes directly to energy content [35]. Hydrogen content also varies, generally mirroring carbon trends, which enhances energy density and flame temperature during. Oxygen content is variable but typically lower than that of carbon and hydrogen, influencing both combustion properties and overall energy content.

Atomic Ratio, similarly, with HY and the HHV, evaluates the effectiveness and quality of hydrochar produced through hydrothermal carbonization (HTC) processes. The highest hydrogen-to-carbon (H/C) ratio is found in raw sewage sludge, which has a value of 1.71. This indicates a high hydrogen content relative to carbon, suggesting a greater potential for producing gaseous byproducts during combustion. As a result, raw sewage sludge has a lower energy density compared to more carbon-rich fuels. Similarly, the highest oxygen-to-carbon (O/C) ratio is also observed in raw sewage sludge, with a value of

0.82. This reflects the presence of significant oxygen-containing functional groups, which are typical of organic materials. A high O/C ratio is associated with lower energy content, indicating that while raw sewage sludge is rich in organic matter, it may not be an efficient fuel source without further processing.

The Van Krevelen diagram, shown in Fig. 6, serves as a significant analytical tool for understanding the chemical composition of organic materials, particularly in the context of biomass conversion processes. This diagram plots the atomic ratios of hydrogen to carbon (H/C) against oxygen to carbon (O/C), allowing for a visual assessment of how different feedstocks and treatment processes affect the elemental characteristics of raw materials and their hydrochar products [36]. The data points represented includes various raw materials such as SS-Raw and CS-Raw, as well as hydrochars produced from these materials through different treatments. Regions highlighted were adopted from the Van Krevelen diagram presented from Burnham [37].

In examining the positions of Raw Sewage Sludge and Coconut Shell (SS-Raw & CS-Raw) on the diagram, it is observed that these raw materials exhibit relatively high O/C ratios, indicative of their oxygen-rich functional groups. This characteristic is typical of fresh biomass, which contains significant amounts of moisture and other volatile compounds. The H/C ratios for these raw materials are also elevated, reflecting their lower degree of carbonization compared to processed materials. Such high ratios suggest that these raw feedstocks are still in a relatively immature state, with potential for further transformation into more stable forms [38].

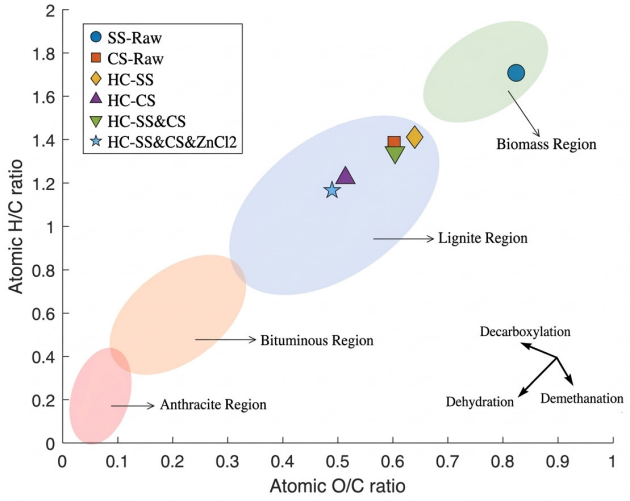

Fig. 6 Van Krevelen diagram showing atomic O/C and H/C ratios of the raw materials and hydrochars

As one transitions to hydrochars from sources such as Sewage Sludge and Coconut Shell (HC-SS and HC-CS), a noticeable shift occurs in both the H/C and O/C ratios. Hydrothermal carbonization (HTC) processes reduce the O/C ratio significantly while also lowering the H/C ratio. This transformation indicates an increase in carbon content and aromaticity, which enhances the energy density and stability of the hydrochars. The shift towards lower ratios shows that the material is maturing as it loses volatile compounds, resulting in a product that contains more carbon and is better suited for different uses, such as energy production or improving soil quality [39]. The diagram also includes data points for treated hydrochars (HC-SS&CS and HC-SS&CS&$ZnCl_2$). The addition of treatments like $ZnCl_2$ can further influence the chemical properties of hydrochars by promoting additional dehydration or carbonization reactions. These treated hydrochars typically exhibit even lower H/C and O/C ratios compared to their untreated counterparts, reflecting enhanced stability and energy content. This aspect is crucial for optimizing biomass conversion methods to produce high-quality fuels or soil amendments.

3.3 Surface functional groups

The surface functional groups of raw materials and hydrochars were determined using FTIR Spectrometer and results are shown in Fig. 7. The presence of hydroxyl groups (–OH) was identified as the cause of peak vibration around 3200–3500 cm^{-1}. This can be observed for the CS raw material and its corresponding hydrochar. In connection, there was no significant changes in the vibrations

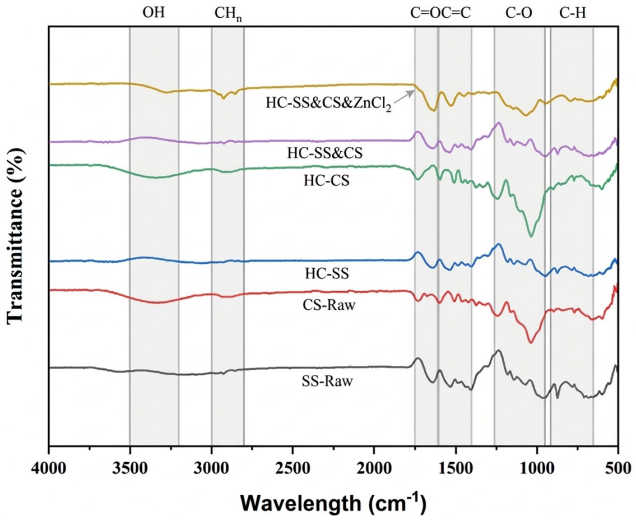

Fig. 7 FTIR spectra of the raw materials, their corresponding hydrochars, co-hydrochar, and $ZnCl_2$-aided

implying that the –OH functional group did not decompose during the hydrothermal carbonization process. Following, the vibration at 2800–3000 cm^{-1} was attributed to aliphatic $–CH_n$ groups [23]. A sharper peak was observed in $ZnCl_2$-aided co-HTC in comparison to the raw materials and other derived hydrochars which is probably because of polymerization. The increase in these aliphatic groups may imply an improve synergistic effect between SS and CS since there was also a peak with the co-HTC but not as strong [7]. On the other hand, similar shapes in hydrochar from CS can be observed while a decline in peak was detected with SS which is because the aliphatic branches broke and became shorter [40]. Next, the vibration at 1610–1750 cm^{-1} was indicative of ketone and esters structures, and C=O bonds of hemicellulose which were mostly related to carbonyl and carboxyl groups. The less intensity of peaks in HTC of SS and co-HTC with CS suggests the decarboxylation reaction [2]. Succeeding is the vibration at 1400–1600 cm^{-1} corresponded to C=C bonds in aromatic compounds, indicating the presence of aromatic compounds in the hydrochar [5]. The peak in $ZnCl_2$-aided co-HTC was enhanced which suggests aromatization and high carbon aromaticity [41].

The vibration near 950–1150 cm^{-1} corresponds to C–O functional groups in cellulose and hemicellulose while up to 1260 are C–O stretching phenols and alcohols [23]. The decrease in vibration for both co-HTC and $ZnCl_2$-aided HTC in comparison to the peaks of the raw materials signifies decomposition of its functional groups [12]. Finally, the range of 915–650 cm^{-1} are the weak absorption peaks of out-of-plane swing vibration of –CH in the benzene ring. The weakened vibration for any of the hydrothermal processes indicates dehydration and decarboxylation reactions [40]. Overall, the presence of zinc chloride in the hydrothermal co-carbonization process enhanced the polymerization and aromatization process thereby increasing its carbon content. Also, increase in aliphatic groups increases HY which can be seen for both the co-HTC process. Furthermore, the synergy between the feedstock slightly increases the dehydration, decarboxylation and aromatization reactions which led to decrease in H/C and O/C ratio.

3.4 Combustion characteristic analysis

The analysis of combustion characteristics through TGA and DTG curves provide critical insights into the thermal behavior of raw materials and hydrochars (Fig. 8). These methods are essential for evaluating the stability and energy potential of biomass feedstocks and their processed forms. In this context, raw materials such as sewage sludge (SS-Raw) and coconut shell (CS-Raw) can be contrasted with hydrochars produced from these feedstocks, including HC-SS and HC-CS, as well as treated hydrochars (HC-SS&CS and HC-SS&CS&$ZnCl_2$). TGA measures the mass loss of a material as it is heated over time, allowing for the identification of decomposition stages and thermal stability. The TGA curves for raw materials typically show multiple weight loss steps, corresponding to the release of moisture, volatile organic compounds and subsequent degradation of organic matter [42]. For raw material sewage sludge (SS-Raw), the TGA curve display significant weight loss at lower temperature, below 200 °C. This initial mass loss is primarily due to moisture evaporation and the release of volatile organic compounds. Embaye et al. [43]

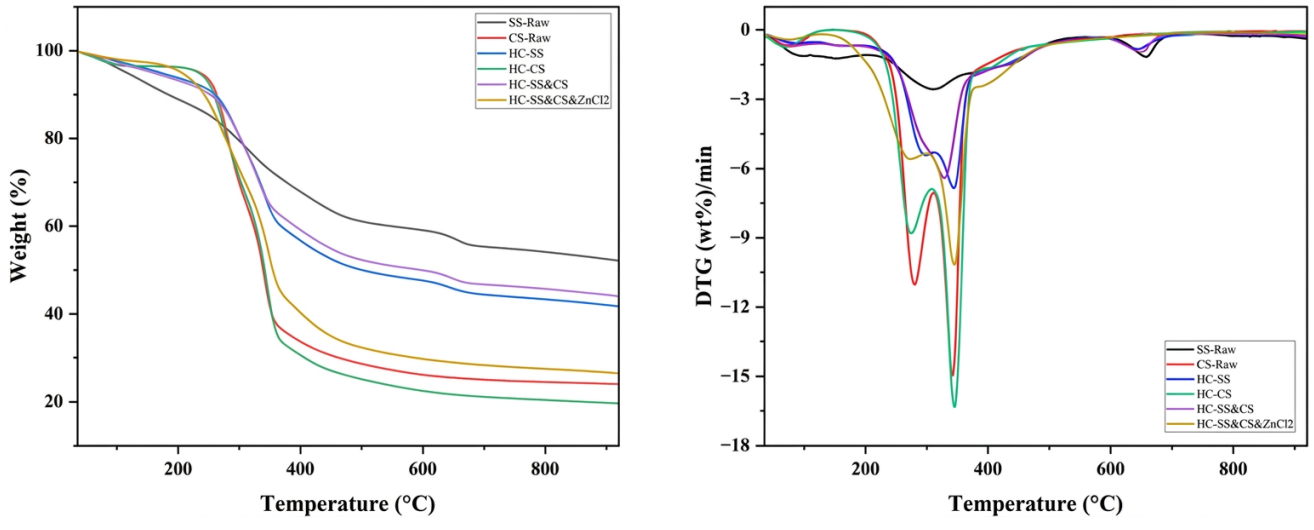

(a) (b)

Fig. 8 (a) TGA and (b) DTG curves of raw materials and hydrochars

found similar results where SS was dried prior the analysis and the decomposition of non-biodegradble and biodegradable organic matters started at lower temperature. In contrast, CS-Raw, being denser and having a higher carbon content, might exhibit a more gradual mass loss, potentially around 10–15%. As biomass undergoes hydrothermal carbonization, the resulting hydrochars such as HC-SS and HC-CS demonstrate altered thermal characteristics. The TGA curves for these hydrochars typically show reduced mass loss at lower temperatures compared to their raw counterparts, indicating enhanced thermal stability.

The DTG curves complement TGA data by providing the rate of mass loss at specific temperatures. Peaks in the DTG curve correspond to the temperatures at which significant decomposition occurs. Hydrochars such as HC-SS and HC-CS typically exhibit sharper peaks at higher temperatures compared to their raw counterparts, reflecting their increased carbonization and reduced volatility. This shift indicates that hydrochars have a higher energy density and are less prone to thermal degradation at lower temperatures, making them more suitable for combustion applications. Treated hydrochars like HC-SS&CS and HC-SS&CS&$ZnCl_2$ may demonstrate even more favorable thermal properties. The addition of $ZnCl_2$ can enhance carbonization, leading to further reductions in mass loss at lower temperatures. These treated materials might display DTG peaks shifted to even higher temperatures. Furthermore, treated hydrochars may display altered thermal characteristics due to chemical modifications that enhance their stability. The presence of additives like $ZnCl_2$ can influence the decomposition behavior by promoting further dehydration or carbonization reactions, which can be observed in both TGA and DTG curves. These treated materials often show improved thermal properties, with reduced mass loss at lower temperatures and higher peak temperatures in DTG curves, indicating enhanced combustion efficiency.

Table 7 presents a comparative analysis of the combustion characteristics of raw materials and their corresponding hydrochars. The comprehensive combustion index was employed to assess the overall combustion behavior of the samples. It was observed that hydrochars, in general, exhibit higher initial combustion temperatures ($T_i s$) compared to their raw material counterparts. This suggests enhanced thermal stability in hydrochars, necessitating higher temperatures to initiate combustion. In contrast, T_i from the hydrochar of CS was reduced by a little which may be due to the formation of C–O functional groups that are volatile. The maximum temperature (T_m) and burnout temperature (T_b) are crucial parameters influencing the combustion process. A lower T_i can potentially lead to spontaneous combustion, posing risks during storage and transportation. Conversely, a higher T_i, as observed in hydrochars, can mitigate such risks.

Moreover, a higher CCI value indicates more vigorous combustion and faster burnout. The results reveal that raw coconut shells and their derived hydrochars exhibit superior combustion properties compared to other materials. The volatile matter content and fixed carbon content significantly impact the combustion process. Coconut shells, with their lower moisture content and higher calorific value, demonstrate favorable combustion characteristics. The higher heat generation during combustion contributes to elevated temperatures, making them suitable for various thermal applications. The analysis of combustion characteristics, particularly the CCI, highlights the potential of hydrochars as valuable energy sources. The enhanced thermal stability and improved combustion kinetics, as evidenced by the higher CCI values, make hydrochars attractive for various applications.

3.5 Synergistic effects

The HY and HHV are important and direct parameters of evaluating the potential of a sample to be an alternative fuel. In Fig. 9, the experimental and calculated values from the co-HTC and $ZnCl_2$-aided co-HTC are presented. From the initial observation, it is clear that the experimental value for co-HTC had a higher value than

Table 7 Combustion characteristics of raw materials and hydrochars

Sample	T_i (°C)	T_m (°C)	T_b (°C)	R_m (% min^{-1})	R_a (% min^{-1})	CCI (10^{-7} min^{-2} $°C^{-3}$)
SS-Raw	128	315	468	−2.57	−1.63	8.16
CS-Raw	239	340	434	−15.03	−5.70	47.67
HC-SS	234	344	467	−6.85	−3.14	11.44
HC-CS	226	346	441	−16.31	−5.68	52.41
HC-SS&CS	230	328	469	−6.40	−2.85	10.56
HC-SS&CS&$ZnCl_2$	189	345	465	−10.19	−4.01	33.29

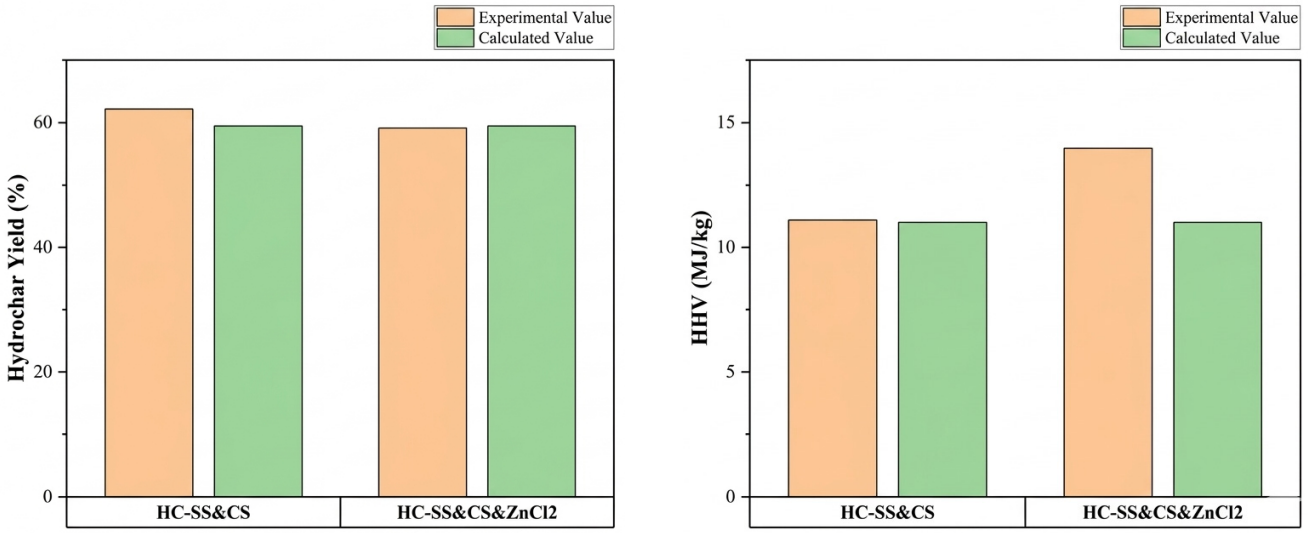

Fig. 9 Effects of co-HTC and zinc chloride-aided co-HTC on (a) hydrochar yield and (b) HHV

the calculated which implies a positive synergistic behavior between the feedstock while the $ZnCl_2$-aided co-HTC shows otherwise. Following the Eq. (7), the synergistic coefficient of co-HTC and $ZnCl_2$-aided co-HTC for HY are 5.35% and −0.61% respectively. Tu et al. [1] found similar results on the improvement of HY from sewage sludge and coconut shell. The addition of coconut shell enhanced the Maillard reaction producing more heterocyclic compounds thus the increase in HY and its brownish and nut-like smell characteristic [44]. The anti-synergistic effect in HY for $ZnCl_2$-aided co-HTC may probably be due to the loss of ash content from the acid-washing procedure or the excessive transformation of volatile matter to the liquid and gas phase.

The synergistic coefficient on the HHV parameter is 0.79% and 27.00% for co-HTC and $ZnCl_2$-aided co-HTC respectively. Tu et al. [1] studied the co-HTC of coconut shells and sewage sludge which focused primarily on its adsorption property, where the result is a positive synergistic coefficient from that parameter. In this study, the HHV of the two raw materials were evaluated and a positive synergistic coefficient was also observed, signifying that the co-HTC of sewage and coconut shells can produce a hydrochar that can be used in different applications and such, effective as an adsorbent and as an alternative fuel. On a different note, there was a significant increase in HHV for the $ZnCl_2$-aided process as also supported by the increase in fixed carbon/carbon content of the sample. The chloride ions from the zinc chloride intensifies the activity of H+ ions from the already acidic HTC process which results in significantly lower pH. This acidity increases the hydrolysis of the macromolecules which then becomes more readily available for dehydration, decarboxylation, Maillard reaction and polymerization which is then attributed to the higher content that relates to the HHV of the sample. Overall, the addition of inorganic binary salt in co-HTC improves the synergistic effect between the two raw materials. This supports the claim of Wang et al. [9], that the synergistic effects of co-HTC between a lignocellulosic material and a protein-non-lignocellulosic material is highly dependent on the strength of the Maillard reaction which is catalyzed in an acidic condition.

4 Conclusion

This study investigates the effectiveness of $ZnCl_2$-aided hydrothermal co-carbonization process to sewage sludge and coconut shells. The process significantly enhanced critical reactions such as dehydration, decarboxylation and aromatization, which improved the fuel properties of the resulting hydrochar. The improved energy density and combustion kinetics make these hydrochars promising alternatives to traditional fuels, contributing to waste management and renewable energy initiatives. Additionally, the outcome of this study was summarized in the following:

- In a $ZnCl_2$-aided co-HTC process, the ratio parameter is deemed as the most significant for both HY and HHV due to the additional organic content of the CS and its synergistic effects. Its strong influence on the process resulted in the insignificance of its interaction effects with temperature and time. For HY, time is considered not significant due to the

acceleration of reactions from the $ZnCl_2$ while temperature is still significant since mass losses from dehydration and decarboxylation may enhance at higher temperatures. Contrarily, the temperature parameter for HHV was not significant while time is significant because of the lowered activation energy.

- Optimization of the co-HTC process using RSM identified the best parameters to achieve a balance between HY and energy content. The optimal conditions were determined to be a 0.66 ratio of SS to CS, a temperature of 180 °C and a residence time of 1.82 h. Under these conditions, the HY was maximized at 56.97% and the HHV reached 13.93 MJ/kg, demonstrating the effectiveness of the optimization process.
- The treatment of raw materials with hydrothermal carbonization process resulted in an increase in FC and increase in fuel ratio. The $ZnCl_2$-aided process further increases the fixed carbon in the co-HTC process signifying an improvement in its fuel quality. Similarly, the carbon content of raw materials was increased with the hydrothermal carbonization treatment along with the lowering of H/C and O/C ratios. $ZnCl_2$-aided co-HTC yielded the highest fuel ratio and lowest H/C and O/C ratio implying its potential as a solid fuel and the effectiveness of $ZnCl_2$ as a catalyst.
- The weak vibrations from the $ZnCl_2$-aided co-HTC process in the –CH group signifies dehydration and decarboxylation while the peak in C=C and $–CH_n$ was a result from aromatization and polymerization. These reactions support the enhanced fuel quality and carbon aromaticity of the hydrochar.
- The combustion characteristics of the hydrochar were significantly improved through the co-HTC process, especially with the aid of $ZnCl_2$. It further enhances hydrochar properties, reducing weight loss at lower temperatures, shifting DTG peaks to higher temperatures, and improving combustion efficiency through increased carbonization and chemical stability. Hydrochars produced in the $ZnCl_2$-aided co-HTC exhibited enhanced thermal stability and superior combustion performance, as evidenced by a composite combustion index of 33.29 (10^{-7} min^{-2} $°C^{-3}$).
- The co-HTC process revealed a clear synergistic interaction between SS and CS, significantly improving the fuel properties of the hydrochar compared to the individual HTC of each feedstock. The co-HTC process without $ZnCl_2$ yielded a modest 0.79% improvement in HHV and with the addition of $ZnCl_2$, this synergistic effect was further amplified, achieving a notable 27% increase in HHV.

Acknowledgement

The researchers would like to express their deepest gratitude to Dr. Rugi Vicente Rubi for his invaluable guidance and expertise as our Research Adviser. We would also like to extend our sincere appreciation to Engr. Jerry Olay for his unwavering support as our Co-Adviser. Their profound knowledge and insightful direction were instrumental in shaping the course of this study and ensuring its successful completion.

Our thanks also go to Engr. Mark Obsid for generously sharing his time and technical proficiency in guiding us through the rigorous testing phase. His expertise was crucial in ensuring the accuracy and reliability of our experimental results. His patience and willingness to answer our questions were greatly appreciated.

We would also like to acknowledge Engr. Albert Evangelista for his assistance and support throughout our laboratory endeavors. His guidance and support were essential in overcoming technical challenges and ensuring the smooth operation of our laboratory experiments.

We are truly grateful for the contributions of everyone who played a crucial role in this journey, reminding us of the collaborative nature of the pursuit of knowledge.

References

[1] Tu, W., Liu, Y., Xie, Z., Chen, M., Ma, L., Du, G., Zhu, M. "A novel activation-hydrochar via hydrothermal carbonization and KOH activation of sewage sludge and coconut shell for biomass wastes: Preparation, characterization and adsorption properties", Journal of Colloid and Interface Science, 593, pp. 390–407, 2021. https://doi.org/10.1016/j.jcis.2021.02.133

[2] He, C., Zhen, Z., Ge, C., Liu, W., Tang, Y., Zhuang, X., Qiu, R. "Synergistic effect of hydrothermal co-carbonization of sewage sludge with fruit and agricultural wastes on hydrochar fuel quality and combustion behavior", Waste Management, 100, pp. 171–181, 2019. https://doi.org/10.1016/j.wasman.2019.09.018

[3] Zhai, Y., Peng, C., Xu, B., Wang, T., Li, C., Zeng, G., Zhu, Y. "Hydrothermal carbonisation of sewage sludge for char production with different waste biomass: Effects of reaction temperature and energy recycling", Energy, 127, pp. 167–174, 2017. https://doi.org/10.1016/j.energy.2017.03.116

[4] Wang, L., Chang, Y., Li, A. "Hydrothermal carbonization for energy-efficient processing of sewage sludge: A review", Renewable and Sustainable Energy Reviews, 108, pp. 423–440, 2019. https://doi.org/10.1016/j.rser.2019.04.011

[5] Cavali, M., Benbelkacem H., Kim, B., Bayard, R., Libardi Junior, N., Gonzaga Domingos, D., Woiciechowski, A. L., Castilhos Junior, A. B. d. "Co-hydrothermal carbonization of pine residual sawdust and non-dewatered sewage sludge – effect of reaction conditions on hydrochar characteristics", Journal of Environmental Management, 340, 117994, 2023. https://doi.org/10.1016/j.jenvman.2023.117994

[6] Cui, D., Zhang, B., Wu, S., Xu, X., Liu, B., Wang, Q., Zhang, X., Zhang, J. "From sewage sludge and lignocellulose to hydrochar by co-hydrothermal carbonization: Mechanism and combustion characteristics", Energy, 305, 132414, 2024. https://doi.org/10.1016/j.energy.2024.132414

[7] Zhao, J., Liu, C., Hou, T., Lei, Z., Yuan, T., Shimizu, K., Zhang, Z. "Conversion of biomass waste to solid fuel via hydrothermal co-carbonization of distillers grains and sewage sludge", Bioresource Technology, 345, 126545, 2022. https://doi.org/10.1016/j.biortech.2021.126545

[8] Wang, Q., Wu, S., Cui, D., Pan, S., Xu, F., Xu, F., Wang, Z., Li, G. "Co-hydrothermal carbonization of corn stover and food waste: Characterization of hydrochar, synergistic effects, and combustion characteristic analysis", Journal of Environmental Chemical Engineering, 10(6), 108716, 2022. https://doi.org/10.1016/j.jece.2022.108716

[9] Wang, Q., Wu, S., Cui, D., Zhou, H., Wu, D., Pan, S., Xu, F., Wang, Z. "Co-hydrothermal carbonization of organic solid wastes to hydrochar as potential fuel: A review", Science of the Total Environment, 850, 158034, 2022. https://doi.org/10.1016/j.scitotenv.2022.158034

[10] Abd Rahman, A. I. M., Bashah, N. A. A., Wan Kamis, W. Z., Isa, N., Osman, M. S., Inderan, V., Olutoye, M. A., Mohd Din, A. T. "Synthesis of Hydrochars via Hydrothermal Carbonization of Zinc Chloride Activated Cotton Textile Waste", Journal of Advanced Research in Fluid Mechanics and Thermal Sciences, 114(2), pp. 196–204, 2024. https://doi.org/10.37934/arfmts.114.2.196204

[11] Multhaupt, H., Bottke, P., Wark, M. "Enhanced Breaking of Lignin and Mesopore Formation in Zinc Chloride Assisted Hydrothermal Carbonization of Waste Biomasses", C, 7(4), 77, 2021. https://doi.org/10.3390/c7040077

[12] Li, F., Zimmerman, A. R., Hu, X., Yu, Z., Huang, J., Gao, B. "One-pot synthesis and characterization of engineered hydrochar by hydrothermal carbonization of biomass with $ZnCl_2$", Chemosphere, 254, 126866, 2020. https://doi.org/10.1016/j.chemosphere.2020.126866

[13] Rosly, M. K. A., Wan Kamis, W. Z., Ali Bashah, N. A., Isa, N., Inderan, V., Mohd Din, A. T. "Effects of $ZnCl_2$ catalyst loading in hydrothermal carbonization of cotton textile waste to produce hydrochars", [pdf] ESTEEM Academic Journal, 19, pp. 10–18, 2023. Available at: https://ir.uitm.edu.my/id/eprint/76043/1/76043.pdf [Accessed: 19 September 2025]

[14] Lu, X., Ma, X., Qin, Z., Chen, X., Chen, L., Tian, Y. "Co-hydrothermal carbonization of sewage sludge and polyvinyl chloride: Hydrochar properties and fate of chlorine and heavy metals", Journal of Environmental Chemical Engineering, 9(5), 106143, 2021. https://doi.org/10.1016/j.jece.2021.106143

[15] Sulaiman, S. M., Nugroho, G., Saputra, H. M., Djaenudin, D., Permana, D., Fitria, N., Putra, H. E. "Valorization of banana bunch waste as a feedstock via hydrothermal carbonization for energy purposes", Journal of Ecological Engineering, 24(7), pp. 61–74, 2023. https://doi.org/10.12911/22998993/163350

[16] Stat-Ease, Inc. "Design-Expert (v7)", [computer program] Available at: https://www.statease.com/software/design-expert/ [Accessed: 19 September 2025]

[17] Minitab, LLC. "Minitab (Version 7)", [computer program] Available at: https://www.minitab.com/en-us/support/downloads/ [Accessed: 19 September 2025]

[18] Amenyeku, G., Cobbina, S. J., Asare, W., Teye, G. K. "Hydrothermal carbonization of organic waste using faecal sludge as a water source: Response surface methodology-Box Behnken design", Environmental Challenges, 15, 100900, 2024. https://doi.org/10.1016/j.envc.2024.100900

[19] Raheem, A., Ding, L., He, Q., Hussain Mangi, F., Hussain Khand, Z., Sajid, M., Ryzhkov, A., Yu, G. "Effective pretreatment of corn straw biomass using hydrothermal carbonization for co-gasification with coal: Response surface Methodology–Box Behnken design", Fuel, 324, 124544, 2022. https://doi.org/10.1016/j.fuel.2022.124544

[20] Shakiba, A., Aliasghar, A., Moazeni, K., Pazoki, M. "Hydrothermal Carbonization of Sewage Sludge with Sawdust and Corn Stalk: Optimization of Process Parameters and Characterization of Hydrochar", BioEnergy Research, 16(4), pp. 2386–2397, 2023. https://doi.org/10.1007/s12155-022-10552-9

[21] ASTM "ASTM D1762-84(2021) Standard Test Method for Chemical Analysis of Wood Charcoal", ASTM International, West Conshohocken, PA, USA, 2021. https://doi.org/10.1520/D1762-84R21

[22] ASTM "ASTM D3172-13(2021)e1 Standard Practice for Proximate Analysis of Coal and Coke", ASTM International, West Conshohocken, PA, USA, 2021. https://doi.org/10.1520/D3172-13R21E01

[23] Cui, D., Zhang, B., Liu, Y., Wu, S., Wang, X., Wang, Q., Zhang, X., Fattahi, M., Zhang, J. "Hydrochar from co-hydrothermal carbonization of sewage sludge and sunflower stover: Synergistic effects and combustion characteristics", Journal of Analytical and Applied Pyrolysis, 183, 106777, 2024. https://doi.org/10.1016/j.jaap.2024.106777

[24] Funke, A., Ziegler, F. "Hydrothermal carbonization of biomass: A summary and discussion of chemical mechanisms for process engineering", Biofuels, Bioproducts and Biorefining, 4(2), pp. 160–177, 2010. https://doi.org/10.1002/bbb.198

[25] Reza, M. T., Lynam, J. G., Uddin, M. H., Coronella, C. J. "Hydrothermal carbonization: Fate of inorganics", Biomass and Bioenergy, 49, pp. 86–94, 2013. https://doi.org/10.1016/j.biombioe.2012.12.004

[26] Sevilla, M., Fuertes, A. B. "The production of carbon materials by hydrothermal carbonization of cellulose", Carbon, 47(9), pp. 2281–2289, 2009. https://doi.org/10.1016/j.carbon.2009.04.026

[27] Kambo, H. S., Dutta, A. "A comparative review of biochar and hydrochar in terms of production, physico-chemical properties and applications", Renewable and Sustainable Energy Reviews, 45, pp. 359–378, 2015. https://doi.org/10.1016/j.rser.2015.01.050

[28] Heilmann, S. M., Davis, H. T., Jader, L. R., Lefebvre, P. A., Sadowsky, M. J., Schendel, F. J., von Keitz, M. G., Valentas, K. J. "Hydrothermal carbonization of microalgae", Biomass and Bioenergy, 34(6), pp. 875–882, 2010. https://doi.org/10.1016/j.biombioe.2010.01.032

[29] Hoseinzadeh Hesas, R., Wan Daud, W. M. A., Sahu, J. N., Arami-Niya, A. "The effects of a microwave heating method on the production of activated carbon from agricultural waste: A review", Journal of Analytical and Applied Pyrolysis, 100, pp. 1–11, 2013. https://doi.org/10.1016/j.jaap.2012.12.019

[30] Bátori, V., Åkesson, D., Zamani, A., Taherzadeh, M. J., Sárvári Horváth, I. "Anaerobic degradation of bioplastics: A review", Waste Management, 80, pp. 406–413, 2018 https://doi.org/10.1016/j.wasman.2018.09.040

[31] Merzari, F., Goldfarb, J., Andreottola, G., Mimmo, T., Volpe, M., Fiori, L. "Hydrothermal Carbonization as a Strategy for Sewage Sludge Management: Influence of Process Withdrawal Point on Hydrochar Properties", Energies, 13(11), 2890, 2020. https://doi.org/10.3390/en13112890

[32] Román, S., Libra, J., Berge, N., Sabio, E., Ro, K., Li, L., Ledesma, B., Álvarez, A., Bae, S. "Hydrothermal Carbonization: Modeling, Final Properties Design and Applications: A Review", Energies, 11(1), 216, 2018. https://doi.org/10.3390/en11010216

[33] Lu, X., Pellechia, P. J., Flora, J. R. V., Berge, N. D. "Influence of reaction time and temperature on product formation and characteristics associated with the hydrothermal carbonization of cellulose", Bioresource Technology, 138, pp. 180–190, 2013. https://doi.org/10.1016/j.biortech.2013.03.163

[34] Vargas-Delgadillo, D. P., Giraldo, L., Moreno-Piraján, J. C. "Preparation and Characterization of Activated Carbon Monoliths with Potential Application as Phenol Adsorbents", Journal of Chemistry, 7(2), pp. 531–539, 2010. https://doi.org/10.1155/2010/672810

[35] Lu, Y., Yang, H., Karasev, A. V., Wang, C., Jönsson, P. G. "Applications of Hydrochar and Charcoal in the Iron and Steelmaking Industry—Part 1: Characterization of Carbonaceous Materials", Sustainability, 14(15), 9488, 2022. https://doi.org/10.3390/su14159488

[36] Wang, S., Wang, Y., Shi, Z., Sun, K., Wen, Y., …, Wang, C.-H. "Van Krevelen diagrams based on machine learning visualize feedstock-product relationships in thermal conversion processes", Communications Chemistry, 6(1), 273, 2023. https://doi.org/10.1038/s42004-023-01077-z

[37] Burnham, A. K. "Van Krevelen Diagrams", In: Sorkhabi, R. (ed.) Encyclopedia of Petroleum Geoscience, Springer, 2018, pp. 1–5. ISBN 978-3-319-02330-4 https://doi.org/10.1007/978-3-319-02330-4_67-1

[38] Ahmad, M., Subawi, H. "New Van Krevelen diagram and its correlation with the heating value of biomass", Research Journal of Agriculture and Environmental Management, 2(10), pp. 295–301, 2013. [online] Available at: https://api.semanticscholar.org/CorpusID:96570932 [Accessed: 19 September 2025]

[39] Braz, C. E., Crnkovic, P. "Physical - Chemical Characterization of Biomass Samples for Application in Pyrolysis Process", Chemical Engineering Transactions, 37, pp. 523–528, 2014. https://doi.org/10.3303/CET1437088

[40] Yang, X., Wang, B., Song, X., Cheng, F. "Evolution characteristics and mechanism of carbon structure during co-hydrothermal carbonization of sewage sludge and sub-bituminous coal", Journal of Cleaner Production, 434, 140382, 2024. https://doi.org/10.1016/j.jclepro.2023.140382

[41] He, C., Giannis, A., Wang, J.-Y. "Conversion of sewage sludge to clean solid fuel using hydrothermal carbonization: Hydrochar fuel characteristics and combustion behavior", Applied Energy, 111, pp. 257–266, 2013. https://doi.org/10.1016/j.apenergy.2013.04.084

[42] Gao, Y., Yu, B., Wu, K., Yuan, Q., Wang, X., Chen, H. "Physicochemical, Pyrolytic, and Combustion Characteristics of Hydrochar Obtained by Hydrothermal Carbonization of Biomass", [pdf] BioResources, 11(2), pp. 4113–4133, 2016. Available at: https://bioresources.cnr.ncsu.edu/BioRes_11/BioRes_11_2_4113_Gao_Physicochemical_Pyrolytic_Combustion_Charact_Hydrochar_Carbonization_Biomass_9070.pdf [Accessed: 19 September 2025]

[43] Embaye, T. M., Ahmed, M. B., Dai, G., Bukhsh, K., Hu, Z., Magdziarz, A., Stojiljkovic, D., Manic, N., Wang, X. "Investigation of thermal behaviour and synergistic effect in co-pyrolysis of municipal solid waste and sewage sludge through thermogravimetric analysis", Journal of the Energy Institute, 111, 101443, 2023. https://doi.org/10.1016/j.joei.2023.101443

[44] Wang, T., Zhai, Y., Zhu, Y., Li, C., Zeng, G. "A review of the hydrothermal carbonization of biomass waste for hydrochar formation: Process conditions, fundamentals, and physicochemical properties", Renewable and Sustainable Energy Reviews, 90, pp. 223–247, 2018. https://doi.org/10.1016/j.rser.2018.03.071